Molecular Catalysis 569 (2024) 114615

Contents lists available at ScienceDirect

Molecular Catalysis

journal homepage: www.journals.elsevier.com/molecular-catalysis

Aerobic Oxidation of Cyclohexane over $LaCo_xFe_{1-x}O_3$ Perovskites in the Liquid Phase☆

Akhil Hareendran [a], Maik Dreyer [b], Takuma Sato [c], Nicolas Cosanne [b], Catalina Leiva Leroy [a], Baoxiang Peng [a,c], Malte Behrens [b], Alexander Schnegg [c], Martin Muhler [a,c,*]

[a] Laboratory of Industrial Chemistry, Ruhr University Bochum, 44780 Bochum, Germany
[b] Institute of Inorganic Chemistry, Kiel University, 24118 Kiel, Germany
[c] Max Planck Institute for Chemical Energy Conversion, 45470 Mülheim an der Ruhr, Germany

ARTICLE INFO

Keywords:
liquid-phase cyclohexane oxidation
free radicals
induction period
cobalt-based perovskites
KA oil selectivity
EPR spectroscopy

ABSTRACT

The aerobic oxidation of cyclohexane is a highly relevant reaction in polymer industry, which generates a mixture of cyclohexanol and cyclohexanone, together known as KA oil. It is further converted to adipic acid, which is used as monomer to produce Nylon-6,6. Herein, we report on the activity of $LaCo_xFe_{1-x}O_3$ perovskites synthesized by co-precipitation with Co contents in the range from $x = 0.00$ to $x = 0.70$. An increase in KA oil selectivity to 95% at a relatively high conversion of 15% compared with the conversion typically used in industry was achieved by increasing the Co content to 0.70. The standard reaction parameters in the three-phase batch reactor were set at 120°C, 1.00 mol/L cyclohexane in 40 mL acetonitrile, 20 mg catalyst, 15 bar O_2, 600 rpm, and 6 h reaction time. In the presence of the $LaCo_{0.7}Fe_{0.3}O_3$ nanoparticles, the apparent activation energy was lowered by 47 kJ/mol to 123 kJ/mol. The kinetic investigation revealed an induction period of 2 h in the uncatalyzed cyclohexane oxidation, which was lowered to less than 1 h by adding the catalyst. A free-radical mechanism was identified by spin-trap EPR measurements where the cyclohexyloxy radical was found to be the main radical. Thus, the cobalt-based perovskite catalysts improve conversion, KA oil selectivity and free-radical generation in the aerobic oxidation of cyclohexane.

1. Introduction

Selective oxidation is a key industrial process to functionalize the C-H bonds of numerous hydrocarbons [1]. Around 20 % of commercially used chemical processes are based on oxidation reactions, producing approximately 600 million tons of chemicals worldwide [2]. The selective oxidation of hydrocarbons leads to commercially valuable chemicals and pharmaceuticals. One of the industrially important reactions is the selective oxidation of cyclohexane with O_2 to cyclohexanol and cyclohexanone (KA oil), which are precursors for the synthesis of Nylon-6,6 via adipic acid [3]. The key challenge is the selective C-H bond activation, which is very stable towards different oxidants requiring elevated temperature and pressure conditions [4]. As of now, the process is carried out in the liquid phase at 120-160°C and 5-15 bar O_2 [5]. Cobalt-based homogenous catalysts such as cobalt (II) naphthenate or cobalt acetyl acetonate are used for this reaction following an auto-oxidation mechanism via the free radicals generated during the process [6]. Heterogenous catalysts such as MoO_3 and Cr_2O_3 are also reported to favor the selective oxidation of cyclohexane [7], but with poor selectivity to KA oil [5-7]. To avoid the formation of a higher carboxylic acid content and to increase the selectivity to KA oil, conversion has been industrially limited to 5-15% [8]. This limitation initiated the development of new heterogenous catalysts, especially iron-based spinels and perovskites, as they are reported to show higher efficiency in a vast range of selective liquid-phase oxidation reactions [9, 10]. The mechanism of cyclohexane oxidation is found to follow different pathways even under the same reaction conditions [11].

Most perovskite metal oxides have found widespread application as heterogeneous catalysts. Perovskites are represented as ABO_3, where A is a cation of a larger size than B with 12 fold coordination filling the voids between the octahedra. Accordingly, the smaller B cations are octahedrally coordinated by oxygen anions, and all six anions at the corners of the octahedra are shared with the six nearest octahedra. Different classes of perovskites are possible depending on the metal ions

☆ Dedicated to Prof. Graham Hutchings

* Corresponding author.
E-mail address: martin.muhler@ruhr-uni-bochum.de (M. Muhler).

https://doi.org/10.1016/j.mcat.2024.114615
Received 13 May 2024; Received in revised form 2 October 2024; Accepted 8 October 2024

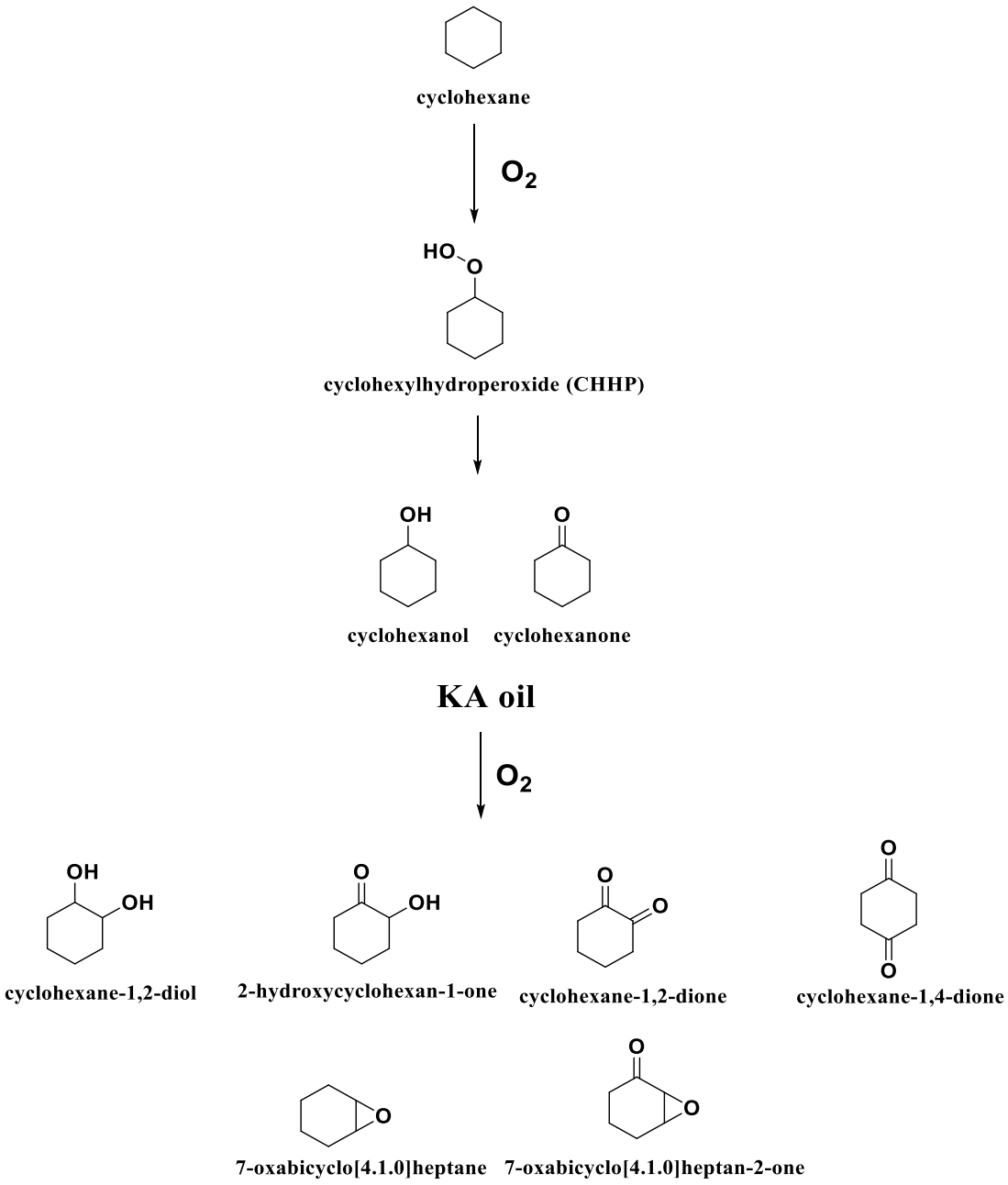

Fig. 1. Observed reaction network for the oxidation of cyclohexane.

used with a broad range of properties. The cation A is generally a lanthanide, alkaline, or alkaline-earth metal, while B is a 3d, 4d or 5d metal. In addition, these metal ions can be also substituted partially like $A_{1-x}A'_xB_{1-x}B'_xO_3$.

Cyclohexane is typically oxidized using molecular O_2 as oxidant at 160°C, 15 bar, and cobalt naphthenate as a homogenous catalyst [12, 13]. The oxidation of cyclohexane primarily leads to the formation of cyclohexyl hydroperoxide (CHHP) and KA oil. The transformation of cyclohexane to CHHP takes place via a radical chain oxidation mechanism, and CHHP undergoes further oxidation yielding KA oil and various other overoxidized products. The challenge in cyclohexane oxidation is to increase both conversion and the selectivity to KA oil, which can be converted to adipic acid by different methods such as oxidation with nitric acid. Alternatively, cyclohexanone can be converted to cyclohexanone oxime and then to caprolactam via the Beckmann rearrangement [14]. Fig. 1 shows an overall reaction scheme for cyclohexane oxidation. Numerous products are possible due to the autoxidation nature of the reaction. The present study focuses on the selective oxidation of cyclohexane to KA oil, which is designated as the primary product. The secondary products shown in Fig. 1 are the ones found in the present study but are not limited to only these.

Cyclohexane oxidation is often reported as a typical example of autocatalytic reactions [15]. The reaction network is vast and follows different pathways under similar reaction conditions. The intermediates

formed during the reaction accelerate the reaction, leading to over-oxidation [16]. Similar to other hydrocarbons, cyclohexane oxidation is also associated with an induction period, during which the free radicals required for initiation are generated [17,18]. The formed cyclohexyl radical ($R^{\bullet}$) combines with molecular oxygen and reacts further with cyclohexane to form the intermediate hydroperoxide (Eqs. 1, 2, and 3).

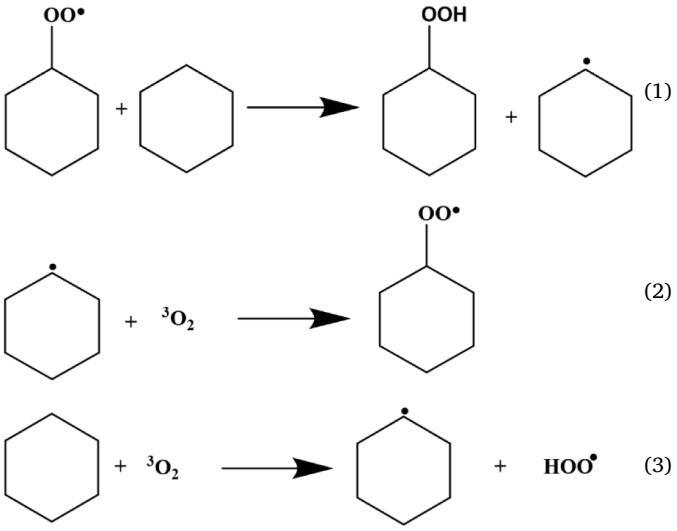

Further decomposition of CHHP leads to the formation of the alkoxy and peroxy radicals (Eq. 4), boosting the reaction rate as the number of free radicals available for propagating the reaction increases. Furthermore, this reaction also results in the formation of water as a coupled product.

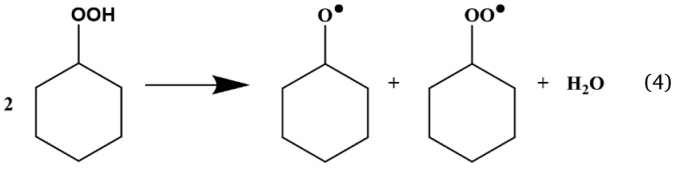

These radicals can then abstract hydrogen from cyclohexane to form the product cyclohexanol and hydroperoxide as shown in Eqs. 5 and 6.

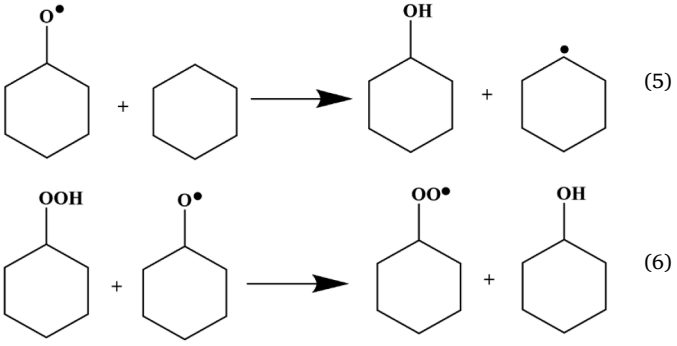

In addition, CHHP can further undergo reaction with the peroxy radical to form the major product cyclohexanone. These reactions are facilitated by the α-H atom at the carbon atom where the carbonyl group is attached. As it is known, the carbonyl group makes the α-H slightly acidic due to its electron-withdrawing nature. This further attracts the relatively dominant peroxy radical to abstract the α-H atom to form cyclohexanone as the major product. This is shown in Eq. 7, where CHHP is again generated together with a hydroxyl radical. However, the hydroxyl radical has two possibilities to further react with CHHP as shown by Eq. 8 and 9. The first reaction (Eq. 8) leads to regeneration of the peroxy radical by abstracting the H atom from the -OOH group, and the second reaction (Eq. 9) proceeds via abstracting the α-H atom to form cyclohexanone. The hydroxyl radical can then participate in the initiation generating more cyclohexyl radicals as shown in Eq. 10. The cyclohexyl radical further reacts with CHHP to form cyclohexanol in Eq. 11. Furthermore, CHHP can also react with cyclohexane to undergo a combination reaction that generates two molecules of cyclohexanol.

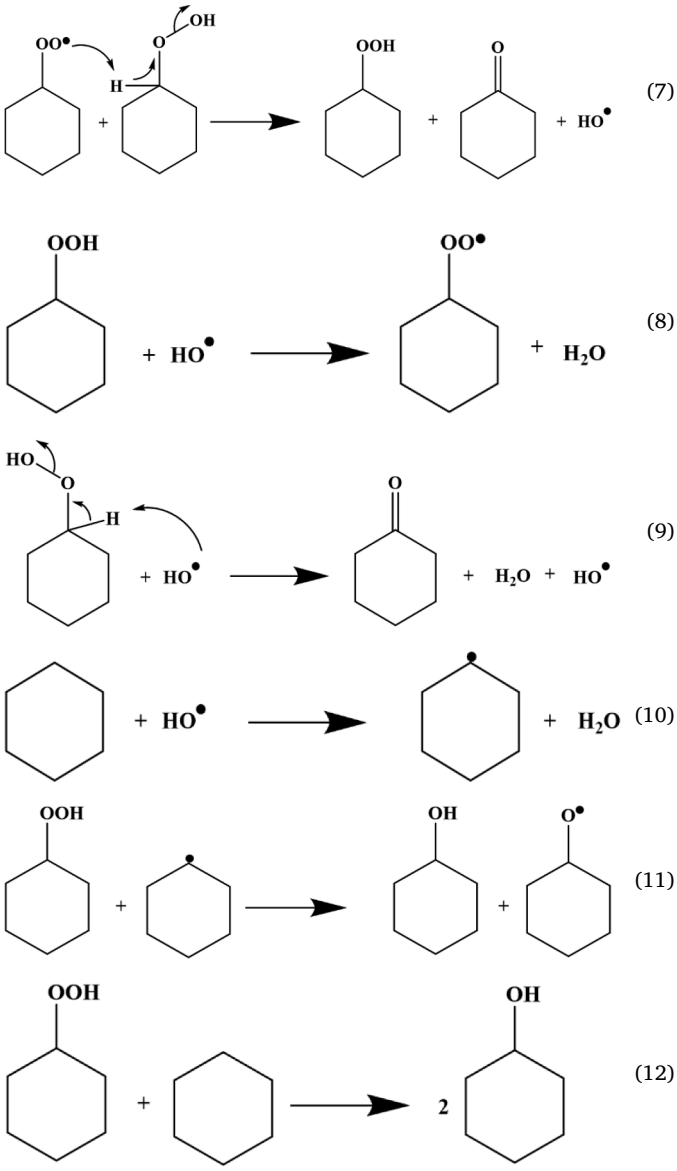

Overall, Eqs. 7-12 explain the low stability of the CHHP intermediate formed. As soon as the intermediate is formed (Eqs. 1-3), it undergoes a wide range of reactions to form cyclohexanone as the main product. Often, it has been assumed that the homolytic O-O cleavage of CHHP is the main source of product formation [5,19,20,21]. However, the reaction network (Equations 7-11) well explains that this is not the case at least in uncatalyzed cyclohexane oxidation. The acidic nature of the α-H atom on the carbon atom bearing the -OOH group is not well discussed in literature. Such an α-H atom abstraction must be assumed to be more attractive to the protophilic free radicals than the O-O homolytic cleavage with high-energy requirements. Upon the introduction of the catalyst, such O-O cleavages could be easily favored in addition to the above reactions. Finally, the peroxy radicals can also undergo recombination leading to a termination reaction, known as Russell termination (Eq. 13).

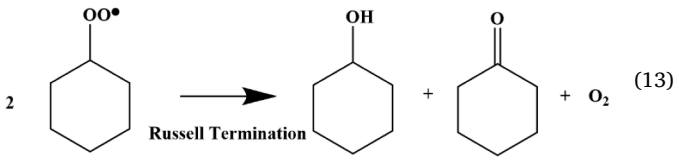

(13)

2. Experimental Section

2.1. Materials

$LaCo_xFe_{1-x}O_3$ perovskites from our previous study [22] were used. For the synthesis of $LaCo_xFe_{1-x}O_3$ perovskites, commercially available regents were utilized, and no additional purification was carried out: lanthanum (III) nitrate hexahydrate (99.9% La, abcr GmbH, Karlsruhe, Germany), iron (III) nitrate nonahydrate (≥ 98%, Sigma-Aldrich GmbH, Germany), cobalt (II) nitrate hexahydrate (≥ 98%, Carl Roth GmbH, Germany), sodium hydroxide (98.5% Carl Roth GmbH, Germany), and sodium carbonate (≥ 99.5%, VWR International GmbH, Germany). Co (II)O was used as a commercial standard (≥ 99.5%, Merck).

2.2. Catalyst Synthesis

The synthesis was performed as part of our previous study and followed the co-precipitation method [22]. The general composition of the perovskite was set as La^{3+}:Co^{2+}:Fe^{3+} = 1:x:(1-x), and x was varied between 0.00 and 0.70. A solution mixture containing 1.2 M NaOH and 0.18 M Na_2CO_3 was used as the precipitating agent. A synthesis setup from Mettler Toledo GmbH consisting of a single-walled glass reactor with a thermostat was used. Isothermal conditions at 10°C and a constant pH of 9.5 maintained through the experiments. Metal salt solution was dosed at a rate of 2.08 g/min with the help of a universal control box. Homogeneity was ensured using an impellor rotating at a rate of 300 rpm. Precipitation was followed by an aging procedure at 10°C for 60 min. The formed precipitate was then isolated by centrifugation (6000 rpm for 2 min). Washing was performed until the supernatant was tested for a conductivity below 0.1 mS/cm. After 12 h drying at 80°C calcination was carried out at 800°C for 3 h.

2.3. Catalyst Characterization

Powder XRD patterns were recorded within a 2θ range of 5° to 90° on a Bruker D8 Advance (Bruker, Billerica, USA) diffractometer equipped with LYNXEYE detector (Ni-filtered CuK_α radiation). Rietveld refinement was carried out using TOPAS software from Bruker, USA for structure analysis and lattice parameter calculations.

N_2 physisorption experiments were performed with a NOVA3000e setup (Quantachrome Instruments, USA) at a temperature of -196°C after degassing at 80°C for 2 h. Brunauer-Emmett-Teller (BET) surface areas were calculated within a relative pressure regime of 0.05 to 0.3.

High-resolution TEM studies were carried out using a JEOL JEM-2800 microscope equipped with Schottky field emission cathode operated at 100-200 kV. A Gatan OneView IS camera recorded the images with a 4K x 4K resolution at 25 fps.

H_2 temperature-programmed reduction (TPR) measurements were carried out using a stainless-steel U-tube reactor and a Hydros 100 thermal conductivity detector. The catalyst was pretreated in 99.99% 50 ml/min He for 1 h at 400°C followed by cooling to 60°C. Then, the reactor was flushed with 50 ml/min 4.58% H_2/Ar (both 99.99%), heated with 10 K/min to 800°C and kept for 1 h at this temperature. Temperature monitoring was performed every 2 s using a thermocouple inside the reactor.

X-ray photoelectron spectroscopy (XPS) was carried out using a Scienta Omicron HiPPLab system equipped with a HiPP-3 APPES analyzer and a high energy resolution monochromator with an Al Ka X-ray source. The spectra were measured with a pass energy of 200 eV and a base pressure of $1{\cdot}10^{-9}$ mbar. The C 1s peak of adventitious carbon was positioned at 284.8 eV to correct for surface charging.

2.4. Cyclohexane Oxidation

For cyclohexane oxidation, a high-pressure stainless-steel reactor 4560 from Parr Instruments was used. The schematic drawing of the reactor used is shown in Fig. 2. In a standard procedure, 1.00 mol/L of cyclohexane was dissolved in 40 mL of acetonitrile (MeCN) with 0.5 mmol of biphenyl as the internal standard. The reaction solution was transferred into the reaction vessel of the stainless-steel reactor, which was then tightened and sealed, followed by flushing with O_2 three times. The O_2 supply to the vessel was then set to 15 bar. Then, the reaction temperature was increased to 140°C for initial studies. After the set temperature had been reached, stirring was switched on with a stirring speed of 600 rpm to initiate the reaction. Two samples each were taken at intervals of 1, 2, 4, and 6 h. One sample was analyzed directly, and the other one was reacted with triphenylphosphine (PPh_3) to convert cyclohexyl hydroperoxide (CHHP) to cyclohexanol. For a typical reaction, an equivalent amount referred to the initial cyclohexane amount of PPh_3 was added to the freshly taken sample at room temperature. The sample was then shaken roughly for 1 min. Shaking led to heat generation, and the sample was ready to be analyzed after cooling. To determine the amount of CHHP formed, the amount of cyclohexanol from the initial sample without PPh_3 had to be subtracted from the sample with PPh_3.

For kinetic investigations, the influences of temperature, pressure, stirring speed, and cyclohexane concentration were studied. The reaction temperatures were set to 100, 110, 120, 130, 140, 150, and 160°C. Since the reaction is autocatalytic, higher temperatures were not chosen, because they may lead to runaway reactions with a wide range of byproducts. The pressure variation included 10, 15, and 20 bar of O_2, and initial concentrations of 0.25, 0.50, 0.75, and 1.00 mol/L cyclohexane were used. Finally, stirring speeds of 500, 600, and 700 rpm were applied. For these variations, an optimum condition of 120°C, 1.00 mol/L cyclohexane, 15 bar O_2, and 600 rpm was set. Under operating conditions, acetonitrile is found to be inert and does not react with the free radicals generated during reaction.

2.5. Gas Chromatography Analysis

A 7820-A GC from Agilent Technologies was used to analyze the samples from the reactions. The GC was equipped with a DB-XLB column (30 m x 180 μm x 0.18 μm) from Agilent and an FID detector. For analysis, 0.6 μL of the samples were injected with a split ratio of 75:1, a split flow of 30 mL/min, and an inlet temperature of 260°C. A standard column run was associated with a He flow of 0.4 mL/min, a pressure of 1.25 bar, and an initial temperature of 80°C. The initial temperature was kept for 3 min and then subsequently heated linearly up to an oven temperature of 140°C with a heating rate of 17°C/min. The end temperature reached 300°C at a heating rate of 20°C/min and was kept for a time interval of 11 min. The result of the GC analysis was quantified using the internal calibration method. An internal standard (biphenyl) was added to the reactant solution beforehand. The relative sensitivity factors (RSF) of all possible reactants and products were calculated by analyzing several solutions with different concentrations of all possible reactants and products. By setting the RSF of biphenyl to 1 and using Eq. 14, the RSF of all other reaction components can be determined.

$$RSF_1 = \frac{n_1}{n_2}\cdot\frac{A_2}{A_1}\cdot RSF_2 \tag{14}$$

where n_i denotes the molar amount of component i, A_i denotes the area of the signal provided by the GC analysis and RSF_i being the relative

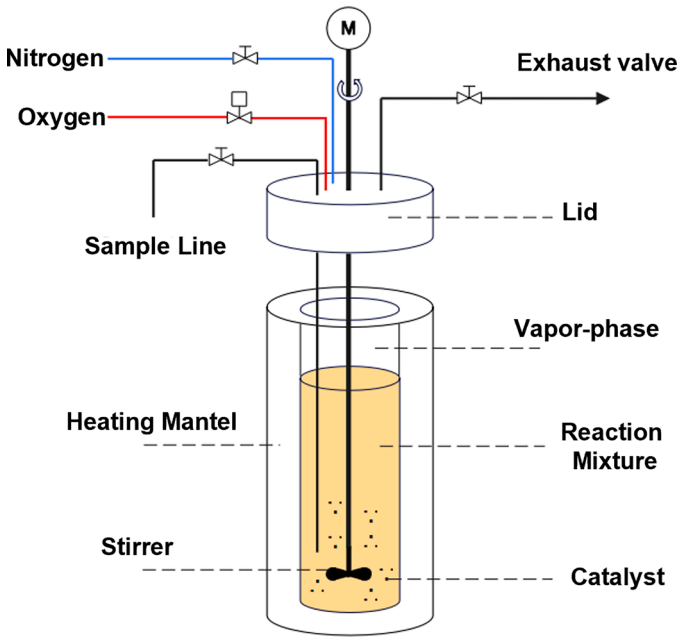

Fig. 2. Schematic drawing of the high-pressure reactor used for cyclohexane oxidation.

sensitivity factor of the component *i*. Initially, a mixture containing cyclohexene, 2-cyclohexene-1-one, 2-cyclohexene-1-ol, cyclohexanol, cyclohexanone, and 1,2-dichlorobenzene (internal standard) in acetonitrile was analyzed by GC. The oven temperature program was varied to determine the analysis conditions for separating all components precisely. At first, a linear heating rate of 12°C/min starting at 100°C was used, and a few signals were missing. Therefore, a second attempt with a lower starting temperature of 80°C was carried out. The heating rate was set to 10°C/min up to 250°C. With this, all signals were visible but two of them were overlapping at a temperature of around 120°C. So, an additional step was inserted into the previous method keeping the temperature for 5 min at 110°C. However, this did not help to separate the signals, and finally, by keeping the starting temperature of 80°C constants for 5 min, the signals were separated. Thus, the oven program was optimized in such a way that the analysis shows sharp signals for all components within a short time of 14 min. For better identification and analysis of the oxidation products, the GC had to be calibrated at a lower conversion range of cyclohexane. Five calibration solutions were prepared with cyclohexane (conversion < 13%) and potential products. Subsequently, five calibrations (calibration A-E) were analyzed and recorded. Thus, the average RSF for all the reaction components was determined from these five calibrations with a standard deviation less than or equal to 0.1. These calibrations and the average values are reported in Table S1.

From the gas chromatogram used, the peak area was used to determine the amount of reactant and product using Eq. 15.

$$n_1 = \frac{A_1}{A_2}\frac{RSF_1}{RSF_2} n_2 \tag{15}$$

From this determined amount, the respective conversion, yield and selectivity was calculated using the following equations:

$$X_i = \frac{n_{i,0} - n_i}{n_{i,0}} \tag{16}$$

$$Y_p = \frac{n_p}{n_{i,0}} \tag{17}$$

$$S_p = \frac{n_p}{n_{i,0} - n_i} \tag{18}$$

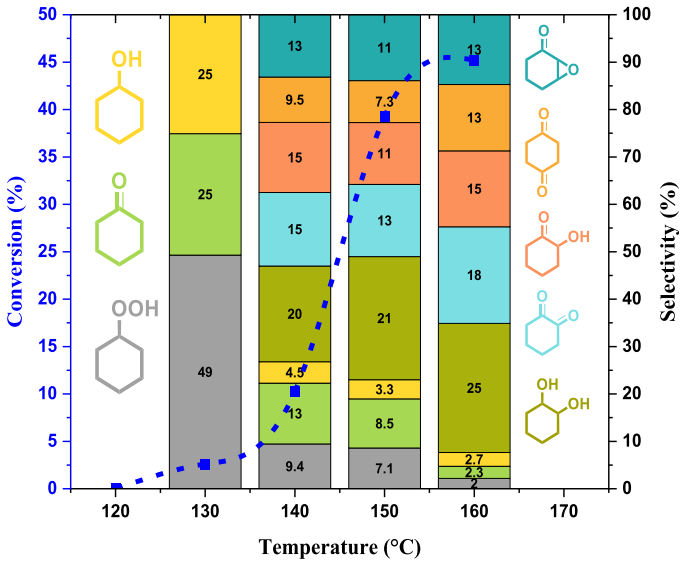

Fig. 3. Effect of temperature on uncatalyzed cyclohexane oxidation after 4 h. Reaction conditions: 0.75 mol/L cyclohexane, 15 bar O_2, 600 rpm, 4 h, acetonitrile as the solvent, and biphenyl as the internal standard. Data points in blue refer to the left Y-axis (conversion) and the data plotted as bar graph refer to the right Y-axis (selectivity). Product order in the bar graph (bottom to top): CHHP, cyclohexanone, cyclohexanol, cyclohexane-1,2-diol, cyclohexane-1,2-dione, 2-hydroxycyclohexan-1-one, cyclohexan-1,4-dione, 7-Oxabicyclo[4.1.0] heptan-2-one.

where X_i is conversion, Y_p is the yield and S_p is the selectivity of product p, $n_{i,0}$ is the initial amount of the reactant cyclohexane, n_i is the amount at a particular interval and n_p is the amount of the product.

2.6. Electron Paramagnetic Resonance (EPR) Spectroscopy

EPR spin-trap measurements using DMPO (5,5-dimethyl-1-pyrroline N-oxide) were carried out to identify the free radicals in the reaction. Initially, a blank measurement was conducted without using DMPO. For this, 1 mL of the reaction mixture was withdrawn at the desired reaction time and transferred to an EPR tube (outer diameter of 1.6 mm and inner diameter of 1.0 mm). After careful cleaning, the filled tubes were placed into the spectrometer and the spectra were recorded. For measurements using DMPO, the reaction samples were withdrawn to a vial with previously weighed 1 mg of DMPO. The mixture was then transferred to the EPR tube after thorough mixing. The measurements were carried out at room temperature using a Bruker Magnettech ESR5000 bench-top EPR spectrometer. The following parameters were used: magnetic field from 332 to 342 mT, modulation amplitude of 0.05 mT, microwave frequency of ~9.46 GHz, and microwave power of 15 mW. To get a better signal to noise ratio, a single scan with a sweep time of 20 s was accumulated 2000 times. All simulations were carried out using the MATLAB toolbox EasySpin [23] with the function "garlic".

2.7. Reusability Studies

Three consecutive reactions were carried out to study the reusability of the catalyst. The standard conditions of 120°C, 1.00 mol/L cyclohexane, 20 mg catalyst, 15 bar O_2, 600 rpm, and 6 h were applied. After each run the catalyst was centrifuged, washed with acetonitrile and dried overnight. The catalyst amount decreased from 20 mg in the first run to 16 mg at the end of the third run.

For ICP-MS measurements, an iCAP RQ ASX-560 instrument was used. The samples were diluted with ultrapure water in a ratio of 1:10. As the addition of water led to opaque solutions, the samples were filtrated. Then, they were acidified with 300µL HNO_3 (supra, 69%) to

Table 1
Derived rate constants in the investigated temperature range.

Temperature (°C)	120*	130	140	150	160
Rate constant k (10^{-3}) [s^{-1}]	-	0.17	0.38	1.48	3.02
R^2	-	0.994	0.991	0.987	0.979

* Reaction at 120°C did not lead to any conversion.

obtain around 2wt% acid concentration in each analyzed solution.

3. Results and Discussion

3.1. Autocatalytic Cyclohexane Oxidation

Uncatalyzed oxidation reactions were carried out prior to adding a catalyst. For the optimization, the reaction parameters were initially set at 140°C, 15 bar O_2 and 0.75 mol/L cyclohexane with acetonitrile as solvent. To determine the reaction order, reactions were carried out using 0.25, 0.50, 0.75, and 1.00 mol/L of cyclohexane at 140°C, 15 bar O_2, and 600 rpm (Figure S1a). Results at this temperature indicate that increasing the cyclohexane concentration above 0.75 mol/L at 140°C favors the secondary products rather than KA oil formation. The average rate of these reactions was determined and plotted against the respective concentrations as shown in Figure S2a. The reaction order is determined as $n = 0.995$ with a regression coefficient of 0.998. Thus, the reaction was observed to follow first-order kinetics. To further determine the rate constants, reactions were carried out at temperatures of 120, 130, 140, 150, and 160°C. The other parameters were kept at 15 bar O_2, 0.75 mol/L of cyclohexane, and 600 rpm.

Fig. 3 shows the overall reaction profile during the temperature variation with respect to cyclohexane conversion and selectivity. The determined rate constants are summarized in Table 1. No products were observed at 120°C. At 130°C, the reaction was found to be slow and associated with an induction period of 3 h for the generation of free radicals required for oxidation. A selectivity of around 25% was obtained for both cyclohexanol and cyclohexanone with a CHHP selectivity of around 50%. Temperatures from 140 to 160°C resulted in an increased reaction rate with an average rate constant of $2.25 \bullet 10^{-3}$ s^{-1}. These reactions were also associated with the formation of byproducts resulting from the overoxidation of KA oil and CHHP. The selectivity of KA oil dropped from 50.4 % to 11.2 % when the reaction temperature was increased from 130 to 160°C. Thus, selectivity depends strongly on conversion: as temperature increases, conversion increases and exceeds the preferred selective regime of below 10%.

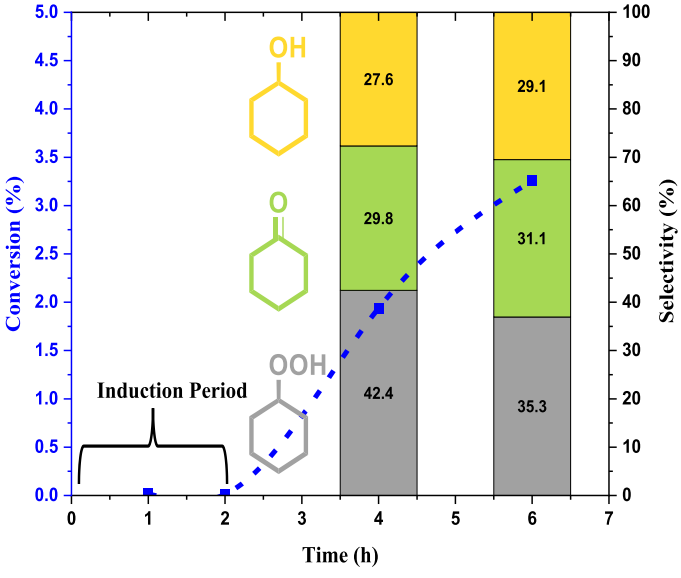

Fig. 4. Uncatalyzed cyclohexane oxidation at 1.00 mol/L cyclohexane and 120°C. Other reaction conditions: 15 bar O_2, 600 rpm, 6 h, acetonitrile as the solvent, and biphenyl as the internal standard. The reaction is associated with an induction period of 2 h. Data points in blue refer to the left Y-axis (conversion) and the data plotted as bars refer to the right Y-axis (selectivity). Product order in the bar graph (bottom to top): CHHP, cyclohexanone, and cyclohexanol.

Figure S2b shows the Arrhenius analysis with a determined apparent activation energy of 170 kJ/mol. To study the effect of O_2 pressure on the autocatalytic cyclohexane oxidation, reactions were carried out at 10, 15, and 20 bar of O_2. As shown in Figure S1b, O_2 did not influence the product selectivity in the uncatalyzed cyclohexane oxidation. However, it did have an impact on cyclohexane conversion: as the O_2 pressure increased, conversion decreased. Therefore, to operate the system in a limited conversion regime, higher O_2 pressures were selected. An increase in pressure from 10 to 20 bar was associated with a lowered conversion by 6% after 4 h. The free radicals produced during initiation are responsible for cyclohexane conversion, and a lower degree of conversion points to a lower number of free radicals at high O_2 pressure. Hence, it can be assumed that the recombination rate of these radicals increases with higher pressure, leading to a lower conversion. The stirring speed of the reaction system was varied to study mass transfer effects. Figure S1c shows the effect of the stirring speed on the oxidation rate of cyclohexane in the range from 500 to 700 rpm, clearly demonstrating that there is no effect of stirring speed on cyclohexane conversion or product selectivity.

To optimize the reaction parameters for catalyzed reactions, the effect of temperature on the uncatalyzed cyclohexane oxidation must be minimized. A relatively low temperature of 120°C was selected for this reason, as homogeneous catalysts are also reported to be active at this temperature [18]. As is evident from Fig. 3, no reaction is observable at 0.75 mol/L and 120°C. Hence, the concentration of cyclohexane was increased to 1.00 mol/L with a prolonged reaction time of 6 h. The conversion-selectivity profile for such a reaction is shown in Fig. 4. No conversion was observed in the first 2 h of the reaction, suggesting an induction period for free-radical formation. After 4 h, a conversion of 1.9% was observed with a KA oil selectivity of 57%, which increased to 60% after 6 h with a conversion of 3.3%. The CHHP selectivity changed from 42% to 35% between the 4th and 6th h of the reaction, suggesting that the decomposition of formed CHHP was not very effective under the applied conditions. However, conversion was doubled after 6 h. Despite

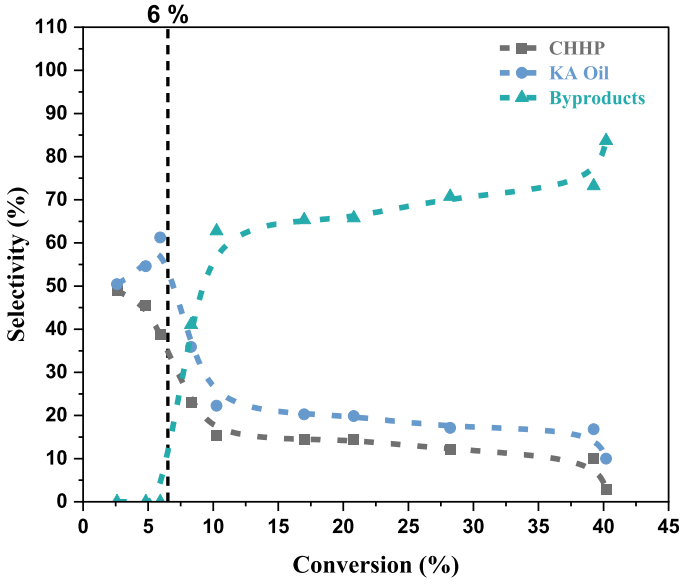

Fig. 5. Conversion-selectivity correlation for the uncatalyzed cyclohexane oxidation.

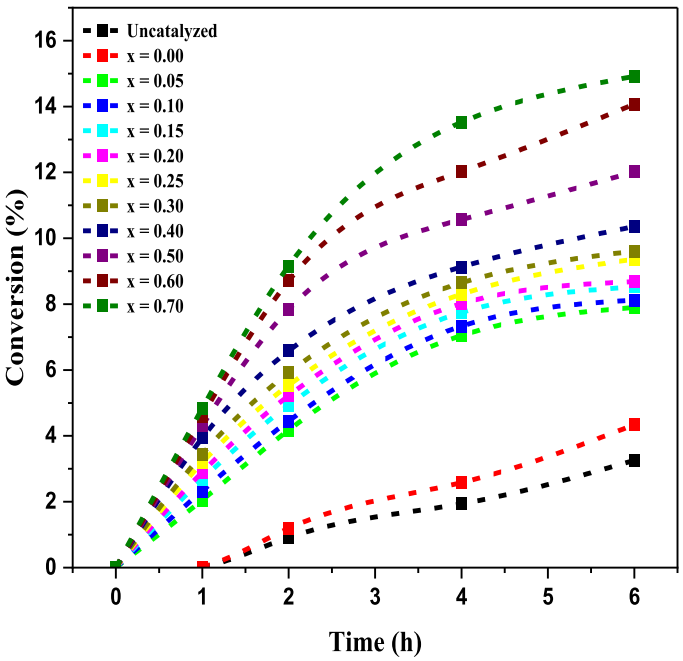

Fig. 6. Conversion-time plots of cyclohexane conversion over the $LaCo_xFe_{1-x}O_3$ catalyst series. Reaction conditions: 120°C, 1.00 mol/L cyclohexane, 20 mg catalyst, 15 bar O_2, 600 rpm, acetonitrile as solvent, and biphenyl as the internal standard.

this increase, KA oil and CHHP selectivity did not change strongly, pointing to an equilibrium between CHHP and KA oil. In comparison to the reactions performed at temperatures in the range from 120 to 160°C, the reaction at 120°C was mildly autocatalytic with KA oil as the only final product. Therefore, the conditions of 120°C, 1.00 mol/L cyclohexane, 15 bar O_2, 600 rpm and 6 h were chosen as optimum parameters for the subsequent kinetic studies in the presence of a catalyst.

Based on the temperature variations from 120 to 160°C, a correlation between cyclohexane conversion and product selectivity was established as shown in Fig. 5. A clear selectivity shift to secondary products is found to occur above 6.5% conversion. This limit at 6.5% is in agreement with the industrial limits as well as the values reported in the literature [5-8]. Therefore, uncatalyzed cyclohexane oxidation is less efficient to produce higher KA oil yields and must be operated in low-conversion regimes. Once conversion reaches around 2.7%, the formed CHHP and KA oil are further oxidized to secondary products. Cyclohexanone may not be converted further as compared to CHHP or cyclohexanol because of its higher stability. Therefore, the key challenge of this study is to design a catalyst that can push the limit to higher degrees of conversion. By employing a catalyst and a suitable temperature, a higher degree of conversion may be achieved, but the effect of temperature on product stability has also to be considered to reduce extensive auto-oxidation.

3.2. *Influence of Cobalt-Based Catalysts on Cyclohexane Oxidation*

3.2.1. *Catalyst Characterization*

The $LaCo_xFe_{1-x}O_3$ perovskite samples synthesized via co-precipitation had been primarily characterized by X-ray diffraction studies (Figure S3) in our previous study [22]. The diffractograms revealed phase segregation at higher Co contents of $x > 0.3$, below which only an orthorhombic perovskite phase was observed. Higher degrees of Co substitution led to the formation of a rhombohedral perovskite phase and a spinel phase which were further confirmed by the Rietveld refinement. The main fraction remained in the orthorhombic/rhombohedral perovskite phase, and only less than 5% was found to be in the spinel phase. N_2 physisorption measurements were used to determine the specific surface areas (7-30 m^2/g) and particle sizes (20-30 nm) (Table S2).

3.2.2. *Catalyst Screening*

The synthesized catalysts were screened for cyclohexane oxidation under the optimized reaction conditions (Fig. 6). The conversion profiles of the catalysts demonstrate relatively high rates with respect to the uncatalyzed reaction. Reaction profiles of the individual catalysts are shown in Figure S4. A 6 h reaction period led to 15.2% cyclohexane conversion for the highest Co content of $x = 0.7$. Without Co ($LaFeO_3$), a similar reaction profile with respect to the uncatalyzed reaction was obtained, where the degree of conversion remained below 4% for the 6 h reaction and an induction period of 1 h was observed. However, a significant increase from 2% to 7% was observed when $x = 0.05$ was introduced. A further Co increase led to higher cyclohexane conversion, which increased more strongly at higher Co contents above $x = 0.3$. The increase in conversion even at a low content of 5% demonstrates the high catalytic activity of Co in these perovskites. The decrease in the induction period (< 1 h) for this Co content also points to the catalytic performance of the exposed Co cations in free-radical generation. Reactions with both $x = 0.6$ and $x = 0.7$ Co reached degrees of conversion between 13.8%-15.3% and are therefore comparable. A phase-pure catalyst with $x = 1$ ($LaCoO_3$) would be desirable for a comparative investigation, but the inevitable phase segregation at higher Co contents leading to a spinel by-phase prevented such a catalyst synthesis using coprecipitation.

Fig. 7 shows the effect of the Co content on the catalytic decomposition of the CHHP intermediate. The Rietveld refinement shown in Figure S3 confirms that the perovskite remains 100% orthorhombic up to $x = 0.3$. Higher substitution levels lead to the transition of the perovskite from orthorhombic to rhombohedral structure. At $x = 0.7$, 62% remains in the rhombohedral structure and 34% in the orthorhombic structure. For 100 % Fe (Co = 0 %, $LaFeO_3$), no decomposition of CHHP was observed. Both the uncatalyzed reaction and $LaFeO_3$ exhibited CHHP formation to a bare minimum of 3% even after 6 h. However, at 5% of Co, the CHHP yield increased to 2.5% within the 1st h and to 3% at the end of the 2nd h, further decreasing to $\leq$ 2.5% after 6 h. CHHP decomposition was insignificant for Co $\leq$ 15%, but with increasing Co content, the formation of this product was promoted. For Co $\geq$ 15%, the CHHP yield increased to above 4% and then decreased considerably beyond 2 h. A higher yield of 6.5% was observed for $x = 0.7$ followed by decomposition to less than 0.5% after 6 h. Thus, the yield profile shows a balance between the formation and decomposition of CHHP when the Co content increases.

The influence of the Co content on conversion and the yields of cyclohexane oxidation products are shown in Fig. 8. With increasing Co content, cyclohexane conversion, the yield of KA oil, and the formation as well as decomposition of CHHP improved. This enhancement is more pronounced for nominal Co contents of 0.4, 0.5, 0.6, and 0.7. For the uncatalyzed reaction (UC), the CHHP and KA oil remain around 3.0% and 1.0% after 6 h, respectively. As the correlation shows, KA oil and CHHP remain relatively the same around 4% and 2.7%, respectively, between Co = 0.05 and Co = 0.2, but still with higher conversion than UC and Co = 0. A gradual increase in KA oil yield was observed from Co = 0.25 to Co = 0.7 with relatively better decomposition of CHHP. A maximum KA oil yield of 13% was achieved for Co = 0.7. A mere CHHP yield of only 0.5% was left after 6 h at this Co content, while conversion was around 14%. Table 2 summarizes degrees of conversion and selectivities reported in literature.

Thus, it can be concluded that the Co content in $LaCo_xFe_{1-x}O_3$ had a strong positive influence on cyclohexane oxidation resulting in higher KA oil yields and faster CHHP decomposition. To ensure that deep oxidation to other products did not take place, the carbon balance was calculated (Table S3). The methods for the product analysis and carbon balance calculation were chosen according to the methodology

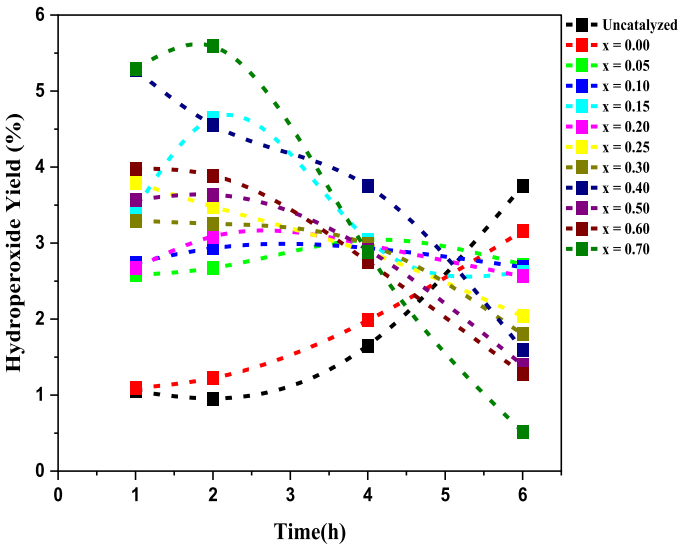

Fig. 7. Influence of the Co content in $LaCo_xFe_{1-x}O_3$ on CHHP formation and decomposition. Reaction conditions: 120°C, 1.00 mol/L cyclohexane, 20 mg catalyst, 15 bar O_2, 600 rpm, acetonitrile as solvent, and biphenyl as the internal standard.

established in literature [33,34,35]. The phase segregation observed in the XRD studies does not seem to have a negative effect on the reaction performance. For Co = 0.7, the orthorhombic perovskite fraction amounted to 34%, the rhombohedral fraction to 62%, and only 5% spinel was found derived from Rietveld refinements [22].

3.2.3. *Kinetic Studies over $LaCo_{0.7}Fe_{0.3}O_3$*

Kinetic investigations were performed using $LaCo_{0.7}Fe_{0.3}O_3$. The standard reaction conditions were kept as 1.00 mol/L cyclohexane, 20 mg catalyst, 15 bar O_2, 600 rpm, 6 h. The temperature effect was initially studied due to its dominant influence on the degree of conversion and the acceleration of the autocatalytic pathway shown in Fig. 9a. At 100°C, hardly any reaction was observed. However, a reaction temperature of 110°C resulted in a 4.9% conversion with a KA oil selectivity of 74.2% and CHHP of 25.2%. The further increase to 120°C led to a faster decomposition of CHHP, decreasing its yield from 25.2% to 7.1% after 6 h reaction. Consequently, an appreciable KA oil selectivity of 92% was achieved at a degree of conversion of about 15%. An Arrhenius analysis as shown in Fig. 9b yielded an apparent activation energy of about 127 kJ/mol. Thus, the $LaCo_{0.7}Fe_{0.3}O_3$ catalyst lowered the apparent activation energy by about 43 kJ/mol.

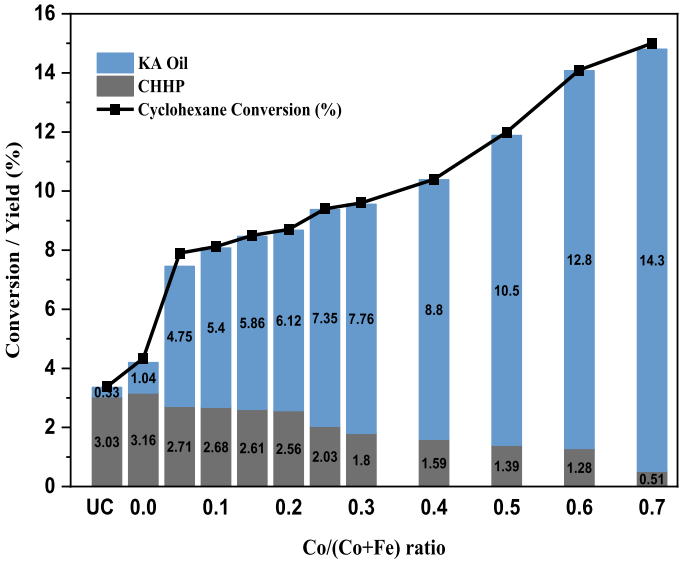

Fig. 8. Influence of Co substitution in the $LaCo_xFe_{1-x}O_3$ perovskite catalysts on cyclohexane conversion and product yield. Reaction conditions: 120°C, 1.00 mol/L cyclohexane, 20 mg catalyst, 15 bar O_2, 600 rpm, 6 h, acetonitrile as solvent, and biphenyl as the internal standard. UC denotes the uncatalyzed reaction. Product order in the bar graph (bottom to top): CHHP and KA oil.

The variation of the initial cyclohexane concentration using 0.25, 0.50, 0.75, and 1.00 mol/L led to an increased conversion (Figure S5a) for the uncatalyzed reaction according to the autocatalytic reaction mechanism outlined by Eqs. (1-6). A faster CHHP decomposition rate was observed when switching from 0.25 mol/L to 1.00 mol/L: at 0.25 mol/L, the CHHP selectivity remained at 24.9% after 6 h compared with 3% when using 1.00 mol/L (Fig. 9a). Hence, there is a balance between the rate of CHHP formation and its decomposition rate. Furthermore, the uncatalyzed reaction was found to follow first-order kinetics as demonstrated in Figure S6. Varying the O_2 pressure from 10 to 20 bar did not influence the product selectivity (Figure S5b). The pressure increase from 10 to 20 bar was associated with a decrease in cyclohexane conversion by 2% after 6 h.

The conversion-selectivity correlation for the catalyzed reaction over $LaCo_{0.7}Fe_{0.3}O_3$ is exhibited in Fig. 10. Compared with the uncatalyzed reaction, KA oil selectivity significantly increased to 90% at a conversion of 12 to 15%, remaining above 85% up to 20% conversion, and then selectivity shifts to byproduct formation. With the introduction of the catalyst, it was possible to lower the reaction temperature to 110°C thereby increasing the stability of the formed KA oil to a certain extent. The lower temperature is expected to lower the rate of overoxidation to the byproducts. However, it is not possible to completely avoid this phenomenon, and at 20.3% conversion, the formation of secondary products is strongly favored.

To identify the generated free radicals, EPR measurements were conducted at room temperature for cyclohexane oxidation over $LaCo_{0.7}Fe_{0.3}O_3$. Radicals belonging to reactive oxygen species such as alkoxy and peroxyl radicals were trapped by DMPO [36,37] forming spin-adducts. Carbon-centered radicals such as alkyl radicals can also be trapped using this approach [38], and distinctive hyperfine coupling constants such as a_N and a_H allow for their identification. Fig. 11 shows the spectra recorded after 6 h of reaction time together with the simulation, which was carried out to elucidate the individual contributions of the different spin-adducts. Four spin-adducts contributions corresponding to cyclohexyloxy ($C_6H_{11}O^{\bullet}$), cyclohexyl peroxy ($C_6H_{11}OO^{\bullet}$), hydroxyl ($HO^{\bullet}$) and cyclohexyl ($C_6H_{11}^{\bullet}$) were identified. In addition, a characteristic contribution of the di-tert-butyl-nitroxide derivative was also obtained, which is associated with the decomposition of DMPO and can be excluded from further discussion. The cyclohexyloxy ($C_6H_{11}O^{\bullet}$) radical was identified as the main radical present during the catalyzed cyclohexane oxidation over $LaCo_{0.7}Fe_{0.3}O_3$ perovskites. Similar studies on cyclohexane oxidation also further confirm this finding [15,16,39,40]. Overall, the liquid-phase oxidation of cyclohexane over $LaCo_{0.7}Fe_{0.3}O_3$ was found to occur via a free-radical mechanism.

Reusability tests using $LaCo_{0.7}Fe_{0.3}O_3$ were performed in three consecutive runs. The conversion-selectivity profile in Fig. 12a shows that the catalyst remained active in all the runs. The selectivity distribution between KA oil and CHHP remained almost the same with KA oil being the main product (≈ 95%). However, the degree of conversion decreased slightly from 15.2% to 13% after the third run. To confirm the structural stability, X-ray diffractograms of the spent catalyst after the third run were compared to the pre-catalyst before reaction. As shown in Fig. 12b, the diffractograms are very similar in their phase composition and intensities indicating high structural stability. The TEM images of the spent catalyst (Fig. 12c) also show that the morphology was not affected by the consecutive runs. Leaching tests were carried out using

Table 2
Conversion and KA oil selectivity reported for cobalt-catalyzed heterogeneous aerobic cyclohexane oxidation.

Catalyst	Temperature (°C)	Oxidizing Agent	Conversion (%)	KA oil Selectivity (%)	Ref.
Present Work	120	O_2	15	95	
$LaCoO_3$	150	O_2	8.3	90	[24]
$La_{0.5}Ca_{0.5}CoO_3$	130	O_2	6.6	83	[25]
Co-PIL-50	130	O_2	20	65	[26]
$CoFe_2O_4/SiO_2$	145	O_2	7.4	95	[27]
Co_3O_4	120	O_2/TBHP	7.6	80	[28]
Au/Al_2O_3	150	O_2	12.6	85	[29]
$CeMn_{0.5}Co_{0.5}O_x$	150	O_2	4.6	68	[30]
CoAlPO	130	Dry Air	8.3	82	[31]
Co-SBA-15	160	O_2	9.4	95	[32]

ICP-MS to check for the stability of the catalysts in the liquid phase. As shown in Table 3, the elemental analysis of the reaction solution resulted in less than 50 parts per billion (ppb) for all ions confirming the high stability of the catalyst. The detection limit according to the used calibration range and dilutions was 50 ppb.

The H_2 TPR profiles obtained with $LaCo_{0.7}Fe_{0.3}O_3$ before and after reaction are shown in Figure S7. The pre-catalyst exhibits two characteristic peaks around 436°C and 845°C. While the former peak is attributed to the reduction of Co^{3+} to Co^{2+}, the latter is assigned to the reduction from Co^{2+} to Co^0. The relative H_2 TPR peak heights show that $LaCo_{0.7}Fe_{0.3}O_3$ contains more Co^{2+} cations after reaction. The expected TPR peaks of Fe^{3+}/Fe^{2+} and Fe^{2+}/Fe^0 (indicated by purple arrows) seem to be masked by the strong Co reduction peaks in agreement with literature [42].

To further investigate the oxidation state of the Co ions in the surface-near region, XPS was applied before and after reaction. The Co 2p spectra are shown in Figure S8 including CoO as reference. For the pre-catalyst, the Co $2p_{3/2}$ and Co $2p_{1/2}$ peaks were observed at 780.3 eV and 795.5 eV, respectively. Clearly, the Co 2p peaks of the spent catalyst are shifted to lower binding energies. For the Co $2p_{3/2}$ peak, a shift of 0.8 eV was found, and the Co $2p_{1/2}$ was shifted by 1.2 eV. These shifts and the satellite structure suggest a more reduced state of the surface-near region of the spent catalyst.

3.3. Discussion

In this work, we demonstrated the catalytic activity of Co cations

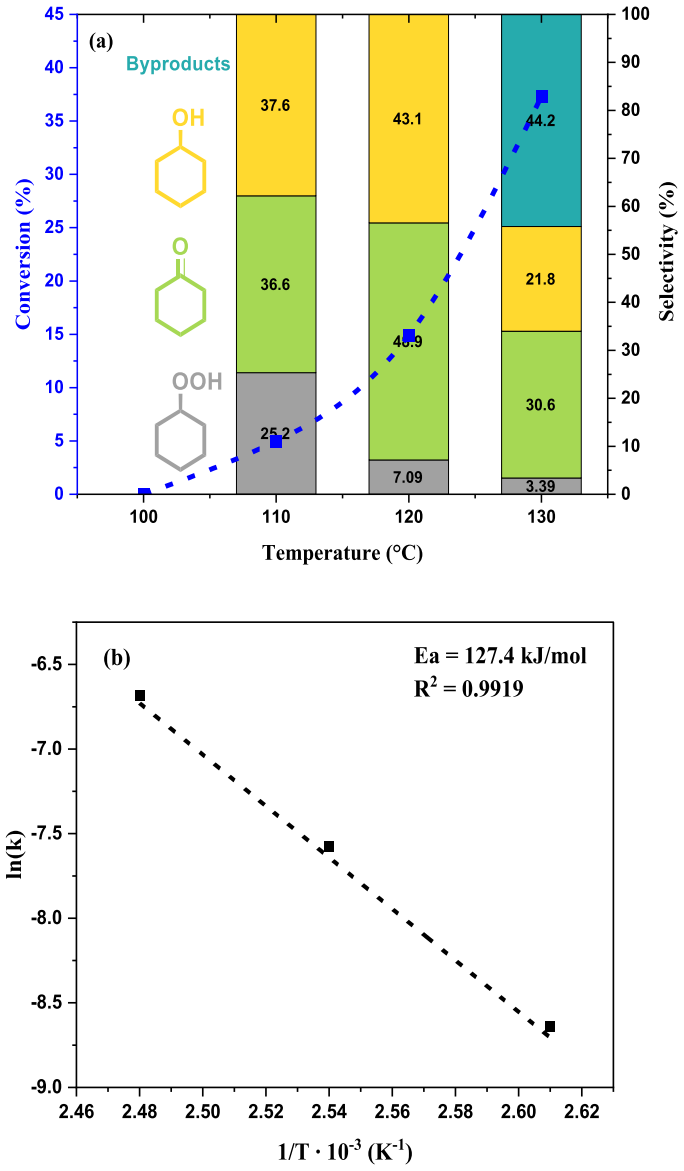

Fig. 9. Kinetic investigations over $LaCo_{0.7}Fe_{0.3}O_3$. (a) Temperature variation from 110 to 140°C and its influence on cyclohexane conversion and product selectivity. The data points in blue refer to the left Y-axis (conversion) and the data plotted as bars refer to the right Y-axis (selectivity). Product order in the bar graph (bottom to top): CHHP, cyclohexanone, and cyclohexanol. (b) Arrhenius plot based on first-order kinetics and the temperature variation.

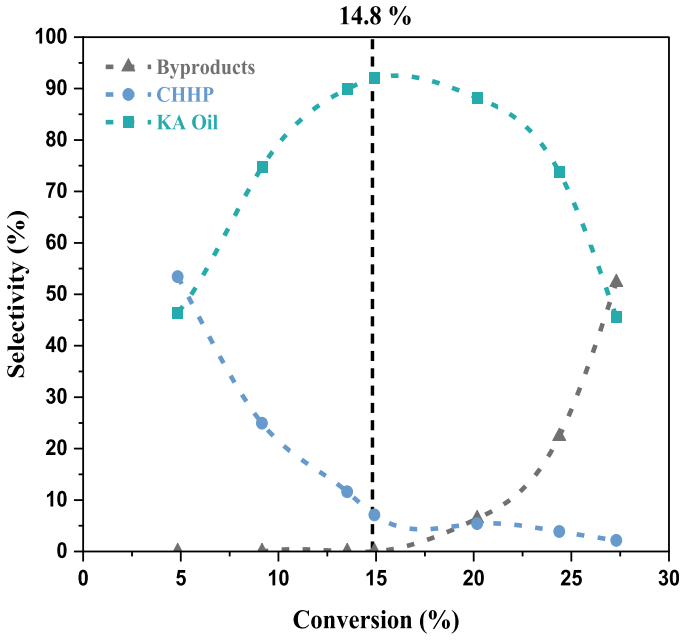

Fig. 10. Conversion-selectivity correlation for cyclohexane oxidation over the $LaCo_{0.7}Fe_{0.3}O_3$ perovskite catalyst. Reaction conditions: 110 - 140°C, 1.00 mol/L cyclohexane, 20 mg catalyst, 15 bar O_2, 600 rpm, 6 h, acetonitrile as solvent, and biphenyl as the internal standard.

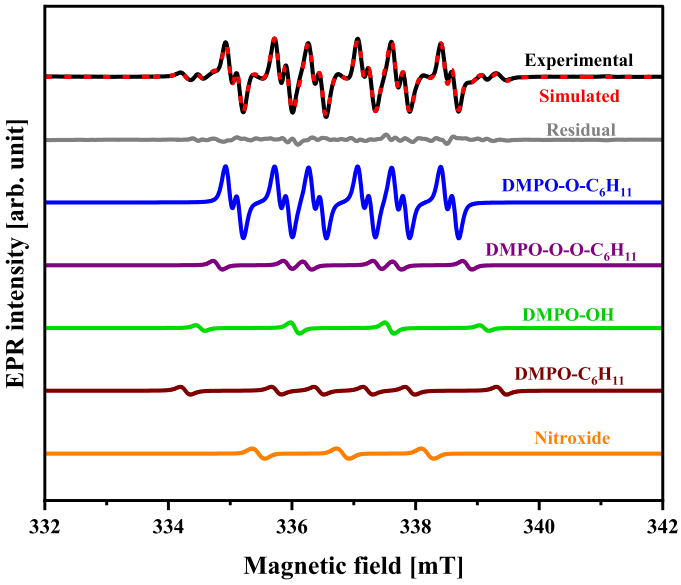

Fig. 11. Experimental (black) and simulated (red) EPR spectra of the DMPO-spin adducts formed after 6 h of cyclohexane oxidation in the presence of $LaCo_{0.7}Fe_{0.3}O_3$. The simulated spectrum is composed of a DMPO–O–C_6H_{11} spin adduct (with a_N = 1.348 mT, $a_{H(\beta)}$ = 0.796 mT, $a_{H(\gamma)}$ = 0.162 mT; 75%; blue) [39], a DMPO–OO–C_6H_{11} adduct (with a_N = 1.454 mT, a_H = 1.142 mT; 7%; purple) [7,8], a DMPO-OH(with a_N = 1.533 mT, a_H = 1.540 mT; 4%; green) [9], a DMPO-C_6H_{11} (with a_N = 1.482 mT, a_H = 2.168 mT; 9%; brown) [40], and a di-tert-butyl-nitroxide derivative (with a_N = 1.372 mT; 9%; orange) [40,41].

substituted into $LaFeO_3$ ($LaCo_xFe_{1-x}O_3$, x = 0-0.7) in the aerobic oxidation of cyclohexane in the liquid phase. An appreciable conversion at a relatively low temperature of 120°C was observed with a higher KA oil selectivity using $LaCo_{0.7}Fe_{0.3}O_3$ as the best catalyst. As shown in Fig. 5, the conversion limit for the uncatalyzed reaction was around 10-12%, above which the primary products cyclohexanol and cyclohexanone further reacted with O_2 forming a variety of secondary products. Such a trend can be accounted for as the characteristics of a consecutive reaction where the faster formation and decomposition of an intermediate species leads to a higher rate of formation of the consecutive species.

As the conversion increased from 2% to 6.5% for the uncatalyzed reaction, the cyclohexyl hydroperoxide selectivity dropped from 50% to 35%, and, consequently, the KA oil selectivity was enhanced from 50% to 65%. Thus, the higher the degree of cyclohexane conversion is, the higher is the hydroperoxide decomposition rate leading to faster KA oil formation. An increase in conversion above 6.5% led to further enhanced KA oil formation and its consecutive overoxidation to byproducts. A further increase in conversion enhanced the KA oil and hydroperoxide decomposition to byproducts, and at a conversion of 10%, the byproducts dominated the reaction with a selectivity of 60%. Thus, the uncatalyzed cyclohexane oxidation is confirmed to proceed via a consecutive reaction pathway.

As shown in Fig. 10, the addition of the catalyst and the lowering of temperature lead to a higher KA oil yield. The key role of the catalyst is demonstrated by the increased KA oil yield at a higher conversion of 15%. Between 15-20% conversion KA oil is highly stable with a selectivity of 95%. Furthermore, the catalyst also contributes to shortening the induction period (Fig. 5).

For the uncatalyzed reaction (Fig. 5), the hydroperoxide decomposition to form KA oil is rather distributed over a minor range of conversion between 2-6%. Above this regime, the formation and decomposition of KA oil is rather instantaneous as shown by the decrease in both hydroperoxide and KA oil selectivity curves. Since KA oil is the consecutive product of the hydroperoxide, an increase in the rate of hydroperoxide decomposition should be followed by an increase in KA oil selectivity. However, here we observe a decrease in both hydroperoxide and KA oil and selectivity, suggesting that the rate constants of the hydroperoxide and KA oil decomposition steps may be similar for the uncatalyzed reaction. Therefore, the formed KA oil is instantaneously overoxidized to further byproducts.

When comparing Figs. 5 and 10, it can be concluded that the catalyst has an active role in enhancing the rate of hydroperoxide decomposition to KA oil. The KA oil selectivity is distributed over a broad conversion

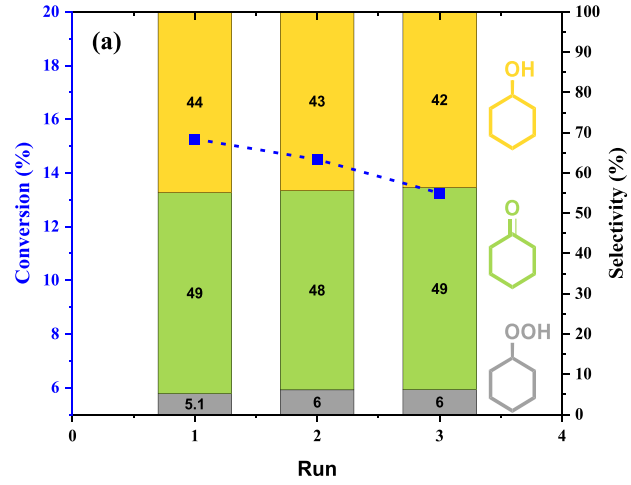

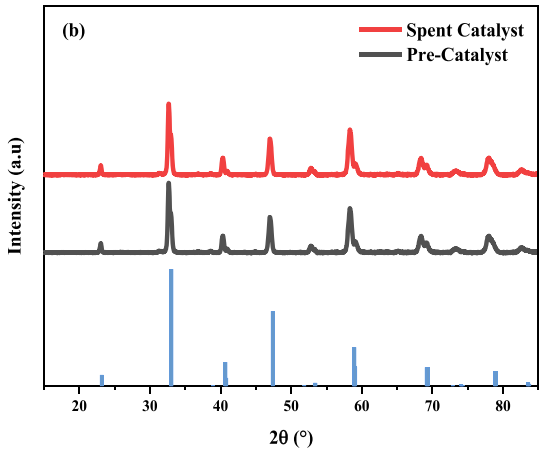

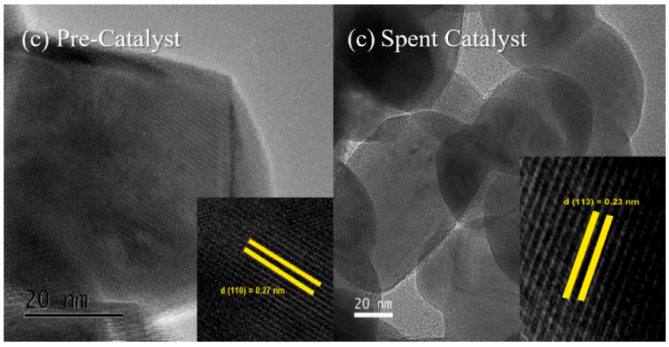

Fig. 12. (a) Reusability test of cyclohexane oxidation over $LaCo_{0.7}Fe_{0.3}O_3$ for three consecutive runs (after 6 h). Reaction conditions: 120°C, 1.00 mol/L cyclohexane, 20 mg catalyst, 15 bar O_2, 600 rpm, 6 h, acetonitrile as solvent, and biphenyl as the internal standard. Data points in blue refer to the left Y-axis (conversion) and the data plotted as bars refer to the right Y-axis (selectivity). Product order in the bar graph (bottom to top): CHHP, cyclohexanone, and cyclohexanol. (b) XRD patterns of $LaCo_{0.7}Fe_{0.3}O_3$ before the reaction (pre-catalyst) and after the consecutive runs (spent catalyst). Reference spectra: ICSD 98-024-7308 (c) TEM images of the catalysts.

Table 3
ICP-MS analysis for the reusability studies over $LaCo_{0.7}Fe_{0.3}O_3$. Minimum detection for quantification was 50 ppb.

Reusability Tests	Amount of La (ppb)	Amount of Co (ppb)	Amount of Fe (ppb)
Run 1	< 50	< 50	< 50
Run 2	< 50	< 50	< 50
Run 3	< 50	< 50	< 50

regime from 5 to 20%, suggesting that the rate constant of hydroperoxide decomposition to KA oil is higher in magnitude compared with the rate constant of KA oil decomposition within this conversion regime. Accordingly, a relatively lower reaction temperature of 120°C may have also contributed to this increase in KA oil selectivity, because the uncatalyzed reactions were observed only above 120°C. Nonetheless, it has to be concluded that the reaction has a characteristic conversion regime, above which the selectivity shift to byproducts takes place. Thus, the catalyst can increase the KA oil stability at relatively higher degrees of conversion compared with the uncatalyzed reaction, but it cannot exclusively favor KA oil formation suggesting that byproduct formation is inevitable at high conversion.

The existence of a free-radical mechanism was proved by the EPR spin-trap investigation. The measurement after 6 h using DMPO confirms that liquid-phase cyclohexane oxidation is occurring via different radicals. Simulation of EPR spectra using existing literature reports identified the cyclohexyloxy radical as the main free radical present in catalyzed reactions. Additionally, cyclohexyl peroxy and cyclohexyl radicals were also identified. The hyperfine coupling constants a_N and a_H were used as the main parameter to differentiate between the radicals. The findings from this spin-trap measurements are also in agreement with the existing literature on catalyzed cyclohexane oxidation in liquid phase [15,16,39,40].

This study confirms that Co ions in $LaCo_xFe_{1-x}O_3$ can enhance both the conversion and selectivity of cyclohexane oxidation to KA oil. Co cations are present in the +3 oxidation state in the perovskite lattice. The characterization studies of $LaCo_xFe_{1-x}O_3$ presented in our previous study (Figure S3) also confirm that Co remains mainly in the +3 oxidation state up to x = 0.7. The Co ions play a vital role in the decomposition of hydroperoxide/peroxide intermediates, as has been frequently reported in oxidation catalysis [43-50]. Co ions are also well studied for the decomposition of H_2O_2 as rationalized by the Haber-Weiss mechanism (Figure S9, S10) [51,52]. Furthermore, Co^{3+} is a more strongly oxidizing agent than Fe^{3+}, which is widely reported in Fenton reactions [51,52]. A plausible explanation is based on the standard oxidation potential of these cations in aqueous solution. As shown in Eq. 19 and 20, Co^{3+} is a strongly oxidizing agent and can easily be reduced to Co^{2+} ions in solution, whereas Fe^{3+} is a relatively weak oxidizing agent.

$$Co^{3+} + e^- \rightarrow Co^{2+},\ E^\circ = +1.808\ \text{V vs. RHE} \quad (19)$$

$$Fe^{3+} + e^- \rightarrow Fe^{2+},\ E^\circ = +0.771\ \text{V vs. RHE} \quad (20)$$

Thus, the high reactivity of Co^{3+} ions in $LaCo_xFe_{1-x}O_3$ finds a parallel in the higher redox potential associated with the Co^{3+}/Co^{2+} redox couple in solution.

As shown in Fig. 13, a plausible pathway could be based on a slightly reduced perovskite surface with localized Co^{2+} cations being exposed. The Co^{3+}-rich perovskite surface is expected to be reduced to localized Co^{2+} species due to the activation of cyclohexane. The activation generates cyclohexyl radicals that further react with O_2 to form the cyclohexyl peroxy radical. Since this species is highly oxidizing in nature, further oxidation of short-lived surface Co^{2+} species takes place, leading to surface regeneration. The homolytic C-H cleavage during this initiation step generates an electron and a proton: Co^{3+} accepts this electron and is reduced to Co^{2+}, and the O^{2-} anion in the catalyst surface is more basic due to the bonding with La^{3+} acting as proton acceptor to become OH^-. This process is known as proton-coupled electron transfer (PCET) and accounts well for the catalyst activation.

The possibilities of CHHP decomposition can be attributed to two different reactions as shown in Fig. 14. There are mainly two pathways involved: (i) the abstraction of the α-H atom from the carbon bearing the hydroperoxyl group or the proton directly from the hydroperoxyl group by a radical (Eqs. 7, 8, and 9), and (ii) the homolytic O-O cleavage of the hydroperoxyl group.

The course of the reaction is mainly controlled by the active species present during the reaction as well as the relative stability of the corresponding radicals or products formed. An uncatalyzed reaction mostly proceeds via the proton abstraction pathway, as the generated peroxy radicals are more thermodynamically stabilized due to resonance stabilization compared with the homolytic O-O cleavage, where the less stable alkoxy radicals are generated. The cyclohexyl peroxy radicals have resonance stabilization resulting from the peroxy group (-O-O•), and therefore the unpaired electron is delocalized within the system and is relatively less available for reaction [53]. Furthermore, the electron

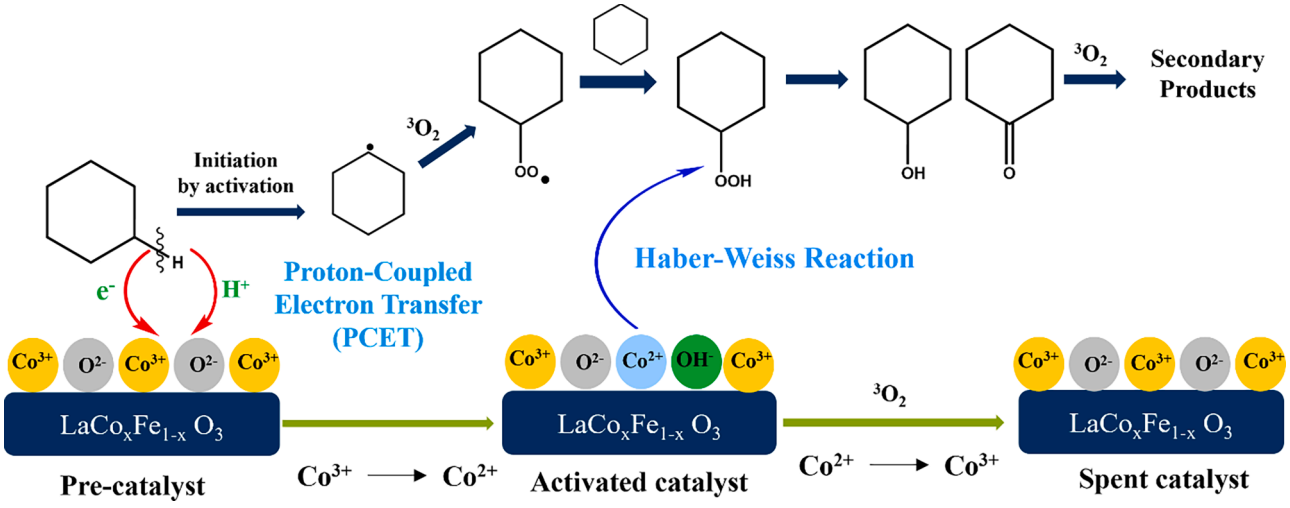

Fig. 13. A plausible reaction pathway based on the surface reduction of Co^{3+} to Co^{2+} ions during the homolytic C-H bond cleavage in cyclohexane. The depiction of the cobalt and oxygen centers is not intended to reflect the actual surface stoichiometry. The less active iron centers have been omitted for the sake of simplicity.

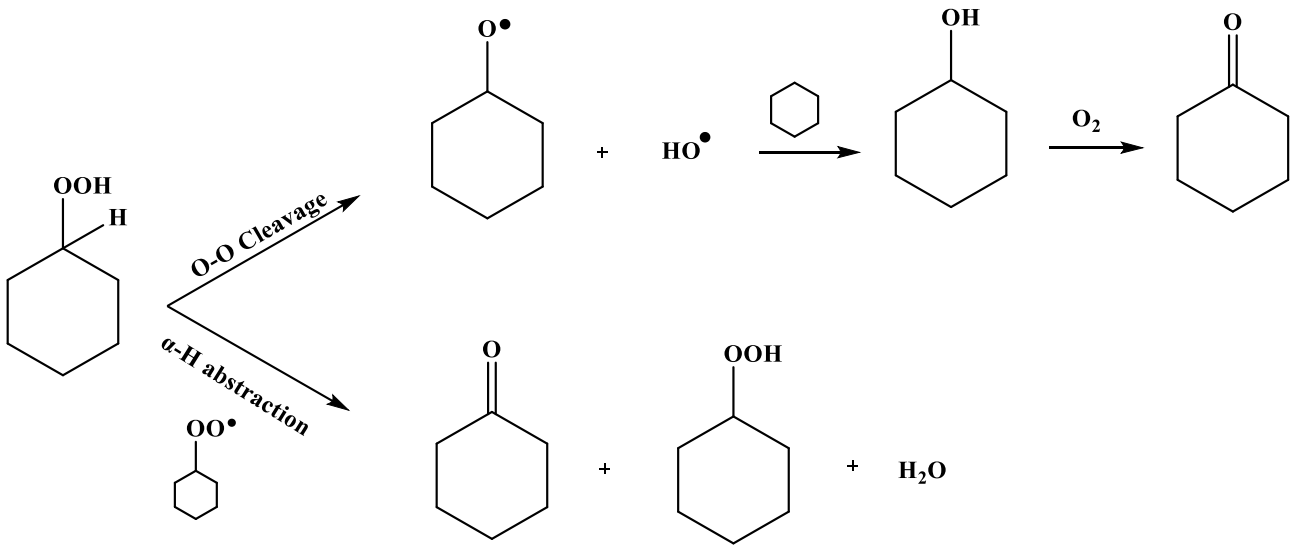

Fig. 14. Reaction pathways for the decomposition of CHHP facilitated via O-O homolytic cleavage and α-H atom abstraction.

density of the nearby C-H bonds can also provide stabilization by hyperconjugation. Even though the O-O bond is significantly weaker due to the strong electron-pair repulsions, its breaking leads to the generation of less stable alkoxy radical. Therefore, the α-H abstraction pathway is preferred to form stable peroxy radicals in the absence of a catalyst. This is also further discussed in kinetic modelling studies where significant attempts were made to quantify the radical formation enthalpy in the gas phase [54]. Due to the mentioned radical stabilization, the enthalpy of formation for the cyclohexyl peroxy radical is lower by 15 kJ/mol compared with the cyclohexyl oxy radical. Furthermore, the enthalpy of formation of the cyclohexyl radical is around 80 kJ/mol higher than that of the cyclohexyl peroxy radical showing the difficulty in initiation by C-H bond activation [54].

Consequently, the short-lived Co^{2+} species catalyzes the decomposition of CHHP by facilitating the homolytic O-O cleavage to form cyclohexanol and cyclohexanone. This route known as Haber-Weiss reaction is often reported in liquid-phase hydrocarbon oxidations involving hydroperoxide intermediates and transition metal catalysts [7,10,43]. Eq. 21 shows the initial step where Co^{2+} facilitates the bond cleavage to form Co(III)-OH species and alkoxy radicals. The Co^{2+} ions are Lewis acids which facilitates the coordination of CHHP molecules to align the peroxy (O-O) bond to the cobalt center. Further reaction generates more radicals as shown in Eq. 22. In radical chain reactions, the termination reactions are rather spontaneous and do not require a catalyst. However, their occurrence can indirectly modulate the concentration of such radicals by influencing the initiation and propagation steps. It could also facilitate radical-radical reactions (termination) by providing coordination sites for the radicals, which brings them to close proximity and increases the feasibility of termination by radical combination.

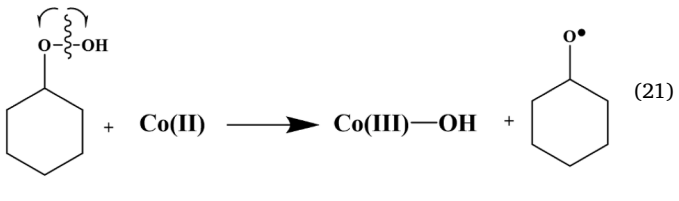

(21)

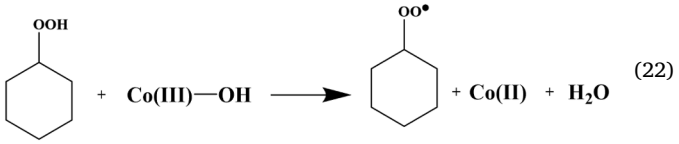

(22)

In further studies, the generated carbon-centered, carboxy, and peroxy radicals will be extensively investigated using radical scavenging coupled with EPR spectroscopy, whereby selective spin traps will be introduced targeting individual radicals.

4. Conclusions

The autocatalytic oxidation of cyclohexane was studied in the liquid phase to analyze the formation kinetics and the stability of KA oil against consecutive overoxidation. Molecular O_2 was used as the oxidizing agent under mild conditions. The uncatalyzed oxidation of cyclohexane to KA oil was found to be conversion-limited and associated with a selectivity shift to other by-products above 6.5% conversion. An induction period of around 2 h was observed for the uncatalyzed reaction at 120°C. A series of $LaCo_xFe_{1-x}O_3$ perovskite catalysts synthesized via co-precipitation was applied in the cyclohexane oxidation to KA oil to enhance the conversion limit and KA oil selectivity. The substitution of Co^{3+} ions into the perovskite lattice of $LaFeO_3$ had beneficial effects on both conversion and KA oil selectivity. Even with a low doping of $x = 0.05$, the conversion-selectivity profile improved significantly, and further stepwise increments of the Co content to $x = 0.7$, boosted the KA oil selectivity to 95% at a higher degree of conversion of 14.8%. In the presence of the $LaCo_{0.7}Fe_{0.3}O_3$ catalyst, the apparent activation energy was lowered by 43 kJ/mol compared with the uncatalyzed reaction. Furthermore, the induction period was shortened to less than 1 h, suggesting a pronounced influence of the exposed Co ions on free-radical generation and favorably increased rates of cyclohexyl hydroperoxide formation and decomposition. Evidence for a free-radical mechanism was provided by spin-trap EPR measurements, which identified the cyclohexyloxy radical as the main radical in catalyzed liquid-phase cyclohexane oxidation. The TPR and the XPS results point to a partial surface reduction under reaction conditions. With this work, we were able to elucidate the catalytic effects of substituting Co^{3+} cations into the $LaFeO_3$ perovskite. A PCET mechanism, in which the Co^{3+} cation serves as the electron acceptor and O^{2-} anion serves as proton acceptor, accounts well for the activation of cyclohexane and of the perovskite catalyst. The decomposition of the hydroperoxide intermediate catalyzed by exposed Co^{2+} cations can mainly occur via the O-O homolytic cleavage or the α-H atom abstraction from the carbon atom bearing the carbonyl group, and the preference for a particular path can be rationalized by the relative stability of the produced carbon-centered oxy and peroxy radicals.

CRediT authorship contribution statement

Akhil Hareendran: Writing – original draft, Visualization, Validation, Methodology, Investigation, Formal analysis, Data curation. **Maik Dreyer:** Visualization, Validation, Methodology, Investigation, Formal analysis. **Takuma Sato:** Writing – review & editing, Visualization, Validation, Methodology, Investigation, Formal analysis. **Nicolas Cosanne:** Writing – review & editing, Visualization, Validation. **Catalina Leiva Leroy:** Writing – review & editing, Visualization, Validation. **Baoxiang Peng:** Writing – original draft, Validation, Supervision, Project administration, Methodology, Investigation. **Malte Behrens:** Writing – review & editing, Validation, Resources, Project administration. **Alexander Schnegg:** Writing – review & editing, Validation, Supervision, Resources, Methodology. **Martin Muhler:** Writing – review & editing, Supervision, Resources, Project administration, Methodology, Investigation, Funding acquisition, Conceptualization.

Declaration of competing interest

The authors declare the following financial interests/personal relationships which may be considered as potential competing interests:

Martin Muhler reports financial support was provided by German Research Foundation. Martin Muhler reports equipment, drugs, or supplies was provided by German Ministry of Education and Research. Martin Muhler reports equipment, drugs, or supplies was provided by Ministry of Culture and Science of the State of North Rhine-Westphalia. If there are other authors, they declare that they have no known competing financial interests or personal relationships that could have appeared to influence the work reported in this paper.

Acknowledgment

This research was funded by the Deutsche Forschungsgemeinschaft (DFG, German Research Foundation, project number - 388390466-TRR 247). We thank Guilong Lu for the TEM measurements. We thank Dr. Wei Xia and Dr. Krishnan Ravi for the XPS measurements. Mrs. Noushin Arshadi is acknowledged for the TPR measurements. This work was supported by the “Center for Solvation Science ZEMOS” funded by the German Federal Ministry of Education and Research BMBF and by the Ministry of Culture and Research of North Rhine-Westphalia.

Supplementary materials

Supplementary material associated with this article can be found, in the online version, at doi:10.1016/j.mcat.2024.114615.

Data availability

Data will be made available on request.

References

[1] G.D. Yadav, R.K. Mewada, D.P. Wagh, H.G. Manyar, Advances and future trends in selective oxidation catalysis: a critical review, Catal. Sci. Technol. 12 (2022) 7245–7269, https://doi.org/10.1039/D2CY01322C.
[2] J. Serrano-Plana, A. Company, M. Costas, O–O Bond Activation in Cu- and Fe-Based Coordination Complexes: Breaking It Makes the Difference. Inorganic Reaction Mechanisms, Elsevier, 2017, pp. 63–105.
[3] A. Abutaleb, M.A. Ali, A comprehensive and updated review of studies on the oxidation of cyclohexane to produce ketone-alcohol (KA) oil, Reviews in Chemical Engineering 38 (2022) 769–797, https://doi.org/10.1515/revce-2020-0059.
[4] N.I. Kuznetsova, L.I. Kuznetsova, N.V. Kirillova, L.G. Detusheva, V.A. Likholobov, M.I. Khramov, J.-E. Ansel, Oxidation of hydrocarbons with dioxygen via peroxide intermediates, Kinet. Catal. 46 (2005) 204–216, https://doi.org/10.1007/s10975-005-0068-x.
[5] S.S. Stahl, P.L. Alsters (Eds.), Liquid Phase Aerobic Oxidation Catalysis: Industrial Applications and Academic Perspectives, Wiley-VCH, Weinheim, Germany, 2016.
[6] M. Nowotny, L.N. Pedersen, U. Hanefeld, T. Maschmeyer, Increasing the Ketone Selectivity of the Cobalt-Catalyzed Radical Chain Oxidation of Cyclohexane, Chem. Eur. J. 8 (2002) 3724–3731, https://doi.org/10.1002/1521-3765(20020816)8:16<3724::AID-CHEM3724>3.0.CO;2-W.
[7] M. Conte, V. Chechik, Spin trapping of radical intermediates in gas phase catalysis: cyclohexane oxidation over metal oxides, Chem. Commun. (Camb) 46 (2010) 3991–3993, https://doi.org/10.1039/C0CC00157K.
[8] H. Jaafar, B. Vileno, A. Thibon, D. Mandon, Tuning the conversion of cyclohexane into cyclohexanol/one by molecular dioxygen, protons and reducing agents at a single non-porphyrinic iron centre and chemical versatility of the tris(2-pyridylmethyl)amine TPAFe(II)Cl2 complex in mild oxidation chemistry, Dalton Trans. 40 (2011) 92–106, https://doi.org/10.1039/C0DT00756K.
[9] J. Büker, B. Alkan, Q. Fu, W. Xia, J. Schulwitz, D. Waffel, T. Falk, C. Schulz, H. Wiggers, M. Muhler, B. Peng, Selective cyclohexene oxidation with O 2 H 2 O 2 and tert -butyl hydroperoxide over spray-flame synthesized LaCo 1−x Fe x O 3 nanoparticles, Catal. Sci. Technol. 10 (2020) 5196–5206, https://doi.org/10.1039/D0CY00906G.
[10] D. Waffel, E. Budiyanto, T. Porske, J. Büker, T. Falk, Q. Fu, S. Schmidt, H. Tüysüz, M. Muhler, B. Peng, Investigation of Synergistic Effects between Co and Fe in Co3-xFexO4 Spinel Catalysts for the Liquid-Phase Oxidation of Aromatic Alcohols and Styrene, Molecular Catalysis 498 (2020) 111251, https://doi.org/10.1016/j.mcat.2020.111251.
[11] A.L. Perkel, S.G. Voronina, Mechanisms of the formation of carboxylic acids and their anhydrides during the liquid-phase oxidation of cyclohexane, Russ Chem Bull 68 (2019) 1478–1498, https://doi.org/10.1007/s11172-019-2582-4.
[12] A.L. Perkel, S.G. Voronina, G.G. Borkina, Liquid-phase oxidation of cyclohexane. Elementary steps in the developed process, reactivity, catalysis, and problems of conversion and selectivity, Russ Chem Bull 67 (2018) 1747–1758, https://doi.org/10.1007/s11172-018-2288-z.
[13] M.A. Andrade, L.M. Martins, Sustainability in Catalytic Cyclohexane Oxidation: The Contribution of Porous Support Materials, Catalysts 10 (2020) 2, https://doi.org/10.3390/catal10010002.
[14] K.T. Zuidhof, M.H.J.M. de Croon, J.C. Schouten, Beckmann rearrangement of cyclohexanone oxime to ε-caprolactam in microreactors, AIChE Journal 56 (2010) 1297–1304, https://doi.org/10.1002/aic.12051.
[15] I. Hermans, P.A. Jacobs, J. Peeters, To the core of autocatalysis in cyclohexane autoxidation, Chem. Eur. J. 12 (2006) 4229–4240, https://doi.org/10.1002/chem.200600189.
[16] D.G. Hendry, C.W. Gould, D. Schuetzle, M.G. Syz, F.R. Mayo, Autoxidations of cyclohexane and its autoxidation products, J. Org. Chem. 41 (1976) 1–10, https://doi.org/10.1021/jo00863a001.
[17] M.F.R. Mulcahy, The oxidation of hydrocarbons. Some observations on the induction period, Trans. Faraday Soc. 45 (1949) 575, https://doi.org/10.1039/TF9494500575.
[18] D. Yang, L. Gao, W. Zhao, Synthesis, Characterization and Catalytic Activity of Dialdehyde Starch-Schiff Base Co(II) Complex in the Oxidation of Cyclohexane, Catal Lett 126 (2008) 84–88, https://doi.org/10.1007/s10562-008-9579-1.
[19] H. Li, Y. She, T. Wang, Advances and perspectives in catalysts for liquid-phase oxidation of cyclohexane, Front, Chem. Sci. Eng. 6 (2012) 356–368, https://doi.org/10.1007/s11705-012-0903-3.
[20] M.A. Andrade, L.M. Martins, Sustainability in Catalytic Cyclohexane Oxidation: The Contribution of Porous Support Materials, Catalysts 10 (2020) 2, https://doi.org/10.3390/catal10010002.
[21] P.R. Makgwane, S.S. Ray, Efficient room temperature oxidation of cyclohexane over highly active hetero-mixed WO3/V2O5 oxide catalyst, Catalysis Communications 54 (2014) 118–123, https://doi.org/10.1016/j.catcom.2014.05.031.
[22] M. Dreyer, D. Cruz, U. Hagemann, P. Zeller, M. Heidelmann, S. Salamon, J. Landers, A. Rabe, K.F. Ortega, S. Najafishirtari, H. Wende, N. Hartmann, A. Knop-Gericke, R. Schlögl, M. Behrens, The Effect of Water on the 2-Propanol Oxidation Activity of Co-Substituted LaFe1-x Cox O3 Perovskites, Chemistry 27 (2021) 17127–17144, https://doi.org/10.1002/chem.202102791.
[23] S. Stoll, A. Schweiger, EasySpin, a comprehensive software package for spectral simulation and analysis in EPR, J. Magn. Reson. 178 (1) (2006) 42–55, https://doi.org/10.1016/j.jmr.2005.08.013.
[24] E. Muhumuza, P. Wu, T. Nan, L. Zhao, P. Bai, S. Mintova, Z. Yan, Perovskite-Type LaCoO3 as an Efficient and Green Catalyst for Sustainable Partial Oxidation of Cyclohexane, Ind. Eng. Chem. Res. 59 (2020) 21322–21332, https://doi.org/10.1021/acs.iecr.0c04095.
[25] X. Li, S. Hao, Z. Chen, T. Huang, S. Fu, F. Zhao, K. You, H. Luo, Roles of the A-Site Ca Dopant in Modifying Surface Properties of a Co-Based Perovskite Catalyst for Selective Oxidation of Cyclohexane, Ind. Eng. Chem. Res. 63 (2024) 6087–6099, https://doi.org/10.1021/acs.iecr.3c04068.
[26] J. Tong, L. Bo, X. Cai, H. Wang, Q. Zhang, L. Su, Aerobic Oxidation of Cyclohexane Effectively Catalyzed by Simply Synthesized Silica-Supported Cobalt Ferrite Magnetic Nanocrystal, Ind. Eng. Chem. Res. 53 (2014) 10294–10300, https://doi.org/10.1021/ie5008213.
[27] L. Zhou, J. Xu, H. Miao, F. Wang, X. Li, Catalytic oxidation of cyclohexane to cyclohexanol and cyclohexanone over Co3O4 nanocrystals with molecular oxygen, Applied Catalysis A: General 292 (2005) 223–228, https://doi.org/10.1016/j.apcata.2005.06.018.
[28] L.-X. Xu, C.-H. He, M.-Q. Zhu, S. Fang, A highly active Au/Al2O3 catalyst for cyclohexane oxidation using molecular oxygen, Catal Lett 114 (2007) 202–205, https://doi.org/10.1007/s10562-007-9058-0.
[29] S. Fu, K. You, W. Ni, Z. Chen, F. Zhao, D. Yan, X. Zhang, H. Luo, One-step highly selective catalytic oxidation of cyclohexane to KA-oil over functional CeMn0.5Co0.5Ox composite oxide: Synergistic effects between Mn and Co species

with different valences and metal ion ratios, Chemical Engineering Science 277 (2023) 118878, https://doi.org/10.1016/j.ces.2023.118878.
[30] Y. Jin, S. Chen, R. Wang, Y. Liu, X. Li, Y. Li, R. Zhang, R. Liu, Selective cyclohexane oxidation enhancement by electronic structures regulation of metal-poly(ionic liquid)s, Green Chemical Engineering 5 (2024) 213–221, https://doi.org/10.1016/j.gce.2023.04.002.
[31] G. Sankar, R. Raja, J.M. Thomas, Catal Lett 55 (1998) 15–23, https://doi.org/10.1023/A:1019093703743.
[32] S. Sreevardhan Reddy, B. David Raju, A.H. Padmasri, P.K. Sai Prakash, K.S. Rama Rao, Novel and efficient cobalt encapsulated SBA-15 catalysts for the selective oxidation of cyclohexane, Catalysis Today 141 (2009) 61–65, https://doi.org/10.1016/j.cattod.2008.04.050.
[33] P. Zhang, H. Lu, Y. Zhou, L. Zhang, Z. Wu, S. Yang, H. Shi, Q. Zhu, Y. Chen, S. Dai, Mesoporous MnCeOx solid solutions for low temperature and selective oxidation of hydrocarbons, Nat. Commun. 6 (2015) 8446, https://doi.org/10.1038/ncomms9446.
[34] S. Chen, Y. Li, Z. Wang, Y. Jin, R. Liu, X. Li, Poly(ionic liquid)s hollow spheres nanoreactor for enhanced cyclohexane catalytic oxidation, Journal of Catalysis 411 (2022) 135–148, https://doi.org/10.1016/j.jcat.2022.05.012.
[35] X. Guo, M. Xu, M. She, Y. Zhu, T. Shi, Z. Chen, L. Peng, X. Guo, M. Lin, W. Ding, Morphology-Reserved Synthesis of Discrete Nanosheets of CuO@SAPO-34 and Pore Mouth Catalysis for One-Pot Oxidation of Cyclohexane, Angew. Chem. Int. Ed Engl. 59 (2020) 2606–2611, https://doi.org/10.1002/anie.201911749.
[36] S. Suzen, H. Gurer-Orhan, L. Saso, Detection of Reactive Oxygen and Nitrogen Species by Electron Paramagnetic Resonance (EPR) Technique, Molecules 22 (2017), https://doi.org/10.3390/molecules22010181.
[37] G.E. Cutsail, Applications of electron paramagnetic resonance spectroscopy to heavy main-group radicals, Dalton Trans 49 (2020) 12128–12135, https://doi.org/10.1039/D0DT02436H.
[38] L. Tian, C.P. Koshland, J. Yano, V.K. Yachandra, I.T.S. Yu, S.C. Lee, D. Lucas, Carbon-Centered Free Radicals in Particulate Matter Emissions from Wood and Coal Combustion, Energy Fuels 23 (2009) 2523–2526, https://doi.org/10.1021/ef8010096.
[39] M. Conte, X. Liu, D.M. Murphy, K. Whiston, G.J. Hutchings, Cyclohexane oxidation using Au/MgO: an investigation of the reaction mechanism, Phys. Chem. Chem. Phys. 14 (2012) 16279–16285, https://doi.org/10.1039/C2CP43363J.
[40] X. Liu, M. Conte, M. Sankar, Q. He, D.M. Murphy, D. Morgan, R.L. Jenkins, D. Knight, K. Whiston, C.J. Kiely, G.J. Hutchings, Liquid phase oxidation of cyclohexane using bimetallic Au–Pd/MgO catalysts, Applied Catalysis A: General 504 (2015) 373–380, https://doi.org/10.1016/j.apcata.2015.02.034.
[41] D. Dvoranová, Z. Barbieriková, V. Brezová, Radical Intermediates in Photoinduced Reactions on TiO2 (An EPR Spin Trapping Study), Molecules 19 (2014) 17279–17304, https://doi.org/10.3390/molecules191117279.
[42] H. Acosta Pérez, C.A. López, O.J. Furlong, M.S. Nazzarro, S.G. Marchetti, L. E. Cadús, F.N. Agüero, Highly Resistant LaCo1−xFexO3 Perovskites Used in Chlorobenzene Catalytic Combustion, Catalysts 13 (2023) 42, https://doi.org/10.3390/catal13010042.
[43] A.L. Perkel, S.G. Voronina, Mechanisms for the formation of ester compounds in the liquid-phase oxidation of cyclohexane, Russ Chem Bull 68 (2019) 1803–1820, https://doi.org/10.1007/s11172-019-2630-0.
[44] T.V. Bukharkina, N.G. Digurov, S.B. Mil'k, A.B. Shelud'ko, Development of the Process of p -Nitroacetophenone and Benzoic Acid Manufacture by the Liquid-Phase Oxidation of Aromatic Compounds, Org. Process Res. Dev. 3 (1999) 404–408, https://doi.org/10.1021/op990030q.
[45] A. Dhakshinamoorthy, E. Montero Lanzuela, S. Navalon, H. Garcia, Cobalt-Based Metal Organic Frameworks as Solids Catalysts for Oxidation Reactions, Catalysts 11 (2021) 95, https://doi.org/10.3390/catal11010095.
[46] I. Arends, R.A. Sheldon, Activities and stabilities of heterogeneous catalysts in selective liquid phase oxidations: recent developments, Applied Catalysis A: General 212 (2001) 175–187, https://doi.org/10.1016/S0926-860X(00)00855-3.
[47] R. Mei, U. Dhawa, R.C. Samanta, W. Ma, J. Wencel-Delord, L. Ackermann, Cobalt-Catalyzed Oxidative C-H Activation: Strategies and Concepts, ChemSusChem 13 (2020) 3306–3356, https://doi.org/10.1002/cssc.202000024.
[48] A.P. Unnarkat, T. Sridhar, H. Wang, S. Mahajani, A.K. Suresh, Cobalt molybdenum oxide catalysts for selective oxidation of cyclohexane, AIChE Journal 62 (2016) 4384–4402. doi:10.1002/aic.15335.
[49] C.W. Anson, S. Ghosh, S. Hammes-Schiffer, S.S. Stahl, Co(salophen)-Catalyzed Aerobic Oxidation of p-Hydroquinone: Mechanism and Implications for Aerobic Oxidation Catalysis, J. Am. Chem. Soc. 138 (2016) 4186–4193, https://doi.org/10.1021/jacs.6b00254.
[50] W.C. Howland, J.B. Gerken, S.S. Stahl, Y. Surendranath, Thermal Hydroquinone Oxidation on Co/N-doped Carbon Proceeds by a Band-Mediated Electrochemical Mechanism, J. Am. Chem. Soc. 144 (2022) 11253–11262, https://doi.org/10.1021/jacs.2c02746.
[51] J. Goldstein, The kinetics of hydrogen peroxide decomposition catalyzed by cobalt-iron oxides, J. Catal. 32 (1974) 452–465, https://doi.org/10.1016/0021-9517(74)90096-7.
[52] J.A. Campbell, Le Châtelier's principle, temperature effects, and entropy, J. Chem. Educ. 62 (1985) 231, https://doi.org/10.1021/ed062p231.
[53] D.A. Pratt, N.A. Porter, Role of hyperconjugation in determining carbon-oxygen bond dissociation enthalpies in alkylperoxyl radicals, Org. Lett. 5 (2003) 387–390, https://doi.org/10.1021/ol027094x.
[54] M. Abbasi, N. Slavinskaya, U. Riedel, Low Temperature Oxidation of Cyclohexane: Uncertainty of Important Thermo-Chemical Properties, Eurasian Chem. Tech. J. 263 (2018), https://doi.org/10.18321/ectj759.